Research Square

Preprints are preliminary reports that have not undergone peer review.
They should not be considered conclusive, used to inform clinical practice,
or referenced by the media as validated information.

Ethylene-Induced Carbohydrate and Hormonal Imbalance Drives Fruitlet Abscission in Coconut (Cocos nucifera L.)

Wenlong Fan
Central South University of Forestry and Technology
Wencheng Fan
Central South University of Forestry and Technology
Linkai Wang
Coconut Research Institute
Liyun Liu
Coconut Research Institute
Meng Li
limeng0422@csuft.edu.cn
Central South University of Forestry and Technology
Jia Li
Coconut Research Institute

Research Article

Keywords: Coconut (Cocos nucifera L.), fruitlet abscission, ethephon treatment, abscission zone, transcriptomics, carbohydraes, endogenous phytohormones

Posted Date: November 25th, 2026

DOI: https://doi.org/10.21203/rs.3.rs-11330417/v1

License: This work is licensed under a Creative Commons Attribution 4.0 International License.
Read Full License

Additional Declarations: No competing interests reported.

Ethylene-Induced Carbohydrate and Hormonal Imbalance Drives Fruitlet Abscission in Coconut (*Cocos nucifera* L.)

Wenlong Fan[1, 2], Wencheng Fan[1, 2], Linkai Wang[2], Liyun Liu[2], Meng Li[1, 3, *], Jia Li[2, *]

Abstract

Background Plant organ abscission is the natural separation of organs such as leaves, flowers, fruits, or seeds from the parent plant. As an adaptive strategy shaped by long-term evolution, it enables plants to regulate nutrient allocation, respond to environmental stresses, and ensure reproductive success. However, excessive fruitlet abscission can severely constrain the yield of *Cocos nucifera* L. In this study, using the abscission-prone cultivar "Wenye No. 2" and exogenous ethephon treatment to simulate the abscission process, we systematically analyzed temporal changes in abscission zone cytology, carbohydrate dynamics, phytohormone profiles, and transcriptomic responses.

Results Soluble sugar levels consistently declined during the abscission process. Regarding phytohormones, ACC (1-aminocyclopropane-1-carboxylic acid) decreased progressively over time, whereas ABA (abscisic acid) and GA (gibberellic acid) increased substantially, IAA (indole-3-acetic acid) dropped markedly, and among the cytokinins, cZ (cis-zeatin) and cZR (cis-zeatin riboside) were significantly higher in ETH (ethephon-treated group) than in CK (control group), whereas tZ (trans-zeatin) and tZR (trans-zeatin riboside) were lower in ETH than in CK. Transcriptome analysis further revealed coordinated upregulation of 33 ethylene-related genes alongside downregulation of the auxin transport genes *PIN1*, *PIN5*, and *PIN6*. WGCNA-based co-expression network

analysis identified multiple hub genes, including ethylene-responsive transcription factors (ERFs) and cell wall hydrolase genes.

Conclusions These findings suggest that ethephon-induced fruitlet abscission in coconut is driven by a concerted action of carbohydrate metabolism impairment, characterized by soluble sugar depletion and starch accumulation, and hormonal imbalance, manifested as ethylene burst and auxin depletion. These changes together trigger transcriptional reprogramming that activates genes involved in cell wall degradation and protective layer formation, ultimately leading to cell separation and fruitlet shedding at the abscission zone. This study provides a theoretical basis for coconut fruit abscission and identifies numerous candidate genes, laying a foundation for fruit tree breeding.

Keywords Coconut (*Cocos nucifera* L.); fruitlet abscission; ethephon treatment; abscission zone; transcriptomics; carbohydraes; endogenous phytohormones.

Background

Fruit abscission is a critical physiological event during plant growth and development and is regulated by a multitude of factors, including both external environmental cues and internal signaling networks [1]. Abscission occurs at specific regions of the plant termed abscission zones (AZs), which primarily encompass four consecutive processes: cell differentiation within the abscission zone, cell wall degradation, organ separation, and formation of the protective layer [2, 3].

Furthermore, this process is coordinately regulated by multiple phytohormones, including auxin (IAA), ethylene, abscisic acid (ABA), gibberellins (GA), jasmonic acid (JA), and cytokinins (CTK) [3]. Extensive studies have demonstrated that abscission is not determined by the absolute level of a single phytohormone, but rather by the dynamic balance among multiple phytohormones, with the antagonistic interplay between IAA and ethylene constituting the core regulatory axis [4]. The complexity of this hormonal balance is primarily manifested at three levels. First, the same phytohormone can exert opposing functions in different species, or even at distinct developmental stages within the same species. For examples, Gibberellins (GA) are generally recognized as abscission suppressors, with exogenous GA_3 application delaying abscission zone formation and reducing cell wall-degrading enzyme activities [5]; however, in rice, higher GA content in the abscission zone correlates with increased abscission susceptibility [6]. Similarly, jasmonic acid (JA) promotes abscission in most plants, through mechanisms such as reducing IAA biosynthesis [7], enhancing cellulase activity [8], or inducing localized cell death in the abscission zone [9]. In contrast, postharvest methyl jasmonate application in peach suppresses ethylene synthesis and thereby delays abscission [10]. Second, phytohormone

functions are concentration-dependent. For instance, cytokinins (CTK) exert differential effects on abscission: downregulation of *GhCKX3* reduces ethylene responsiveness and delays abscission in cotton [11], whereas high-concentration BA treatment in carnation inhibits abscission by blocking the conversion of ACC to ethylene [12]. Third, hierarchical regulatory relationships exist among phytohormones. Abscisic acid (ABA) does not directly induce abscission but rather acts indirectly by suppressing IAA transport and promoting ethylene production [13]. Likewise, IAA not only directly delays abscission but also attenuates the sensitivity of abscission zone cells to ethylene, thereby retarding the abscission process [14]. In abscission-prone soybean varieties, impaired polar auxin transport occurs concomitantly with elevated ABA content, further corroborating the antagonistic relationship between these two phytohormones [15].

As the terminal effector of abscission, ethylene activates the transcription of hydrolase genes, leading to degradation of the abscission zone cell wall [16]. Concurrently, ethylene can reduce bioactive IAA levels by inhibiting polar auxin transport or promoting auxin conjugation, thereby facilitating abscission [17]. In *Paeonia Itoh*, *IpAUX1* enhances cellular responsiveness to ethylene by modulating the auxin gradient across the abscission zone, thereby promoting petal abscission [18]. Carbohydrate deprivation also constitutes a critical factor inducing abscission: in *Glycine max*, carbohydrate starvation induces ABA accumulation and triggers abscission [15]; in litchi, fruitlet abscission occurs when glucose concentrations fall below a critical threshold, with carbohydrate shortage significantly accelerating fruit drop [16]; and in citrus, 3,5,6-Trichloro-2-pyridyloxyacetic acid (3,5,6-TPA) induces fruitlet abscission by reducing carbohydrate supply to the fruit [19].

Beyond phytohormone signaling, transcription factors constitute another critical layer of

regulatory control over organ abscission. The functional characterization of these regulators has been most extensively documented in woody perennials, where lineage-specific transcription factors have emerged as key determinants of abscission timing and efficiency. In litchi, for example, *LcHB2* promotes fruitlet abscission by directly activating cellulase genes [20], whereas LcARF5 regulates the *LcIDL1–LcHSL2* complex to control fruitlet abscission [21]. In *Areca catechu* L, *AcERF116* exerts its function through a dual mechanism: it both modulates hydrolytic enzyme activities within the fruit abscission zone (FAZ) and, via physical interaction with *AcDOF4*, represses *AcPILS7* expression to disrupt polar auxin transport [14, 22]. Beyond these species-specific regulators, the MADS-box family appears to play a more general role, having been implicated in abscission zone formation and development across diverse taxa [23]. Notably, several other transcription factor families, including WRKY [24], MYB [25], and bHLH [26], have also been reported to participate in this process. Collectively, these observations point to a complex and phylogenetically conserved transcriptional landscape that integrates developmental cues with environmental signals to orchestrate organ shedding.

Coconut (*Cocos nucifera* L.) is an economically important crop, yet excessive fruitlet abscission constitutes a critical factor leading to substantial yield reduction, representing a "bottleneck" issue that urgently requires resolution in the industry. In a coconut inflorescence, only about one-third of the initial female flowers develop into mature nuts, with the most severe premature fruit drop occurring at 2–4 months after anthesis, accounting for approximately 44.00% of the total loss[27]. To date, most studies on fruit abscission have focused on species such as litchi and tomato, with limited reports available for coconut. Therefore, elucidating the regulatory mechanisms underlying fruitlet abscission in coconut at both physiological and molecular levels

will facilitate the improvement of fruit set regulation through optimized management of the fruit–tree–environment relationship. The findings of this study will not only enrich our understanding of the regulatory mechanisms governing plant organ abscission but also provide a theoretical basis for improving fruit drop management practices and for molecular breeding in coconut.

Results

Natural and Ethephon-Induced Fruitlet Abscission in Coconut

To simulate the process of premature fruit drop, we sprayed ethephon onto the fruitlets. The treatment induced near-complete abscission, while the control group showed no significant fruit drop (Fig. 1A). In the non-abscised fruits, the fruitlets remained firmly attached to the pedicel (Fig. 1B); in contrast, the abscission zone of the dropped fruits exhibited pronounced specialization and had detached from the pedicel (Fig. 1C). Abscission rates were recorded for both groups at day 0, as well as at 2-and 4-day post-treatment. The results showed that by day 4 after ethephon treatment, the fruitlet abscission rate reached 75.00%, compared with only 12.50% in the control group (Fig. 1D). A significant positive correlation was observed between ethylene levels and abscission rates.

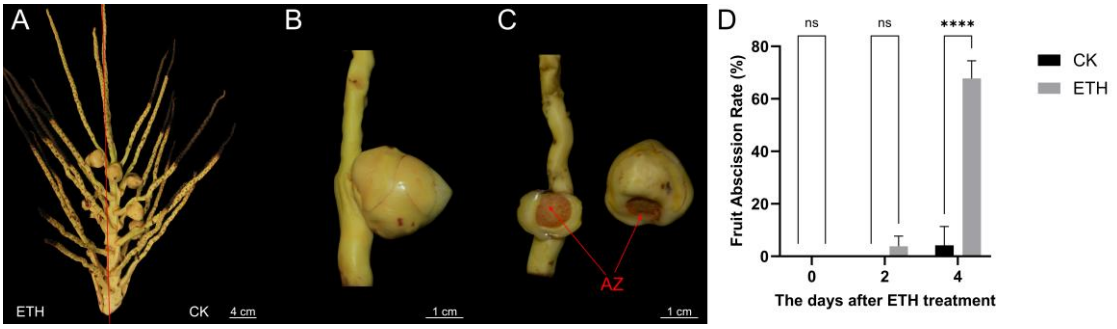


Fig. 1. Morphological characteristics of the abscission zone and fruitlets in coconut.

A Comparison of inflorescences treated with water (CK) or ethephon (ETH); **B** Non-abscised fruitlet; **C** Abscised fruitlet; **D** Abscission rate of coconut fruitlets. **** indicates significant differences from the CK group at $P<0.0001$ (Student's *t*-test). Error bars represent standard deviation (SD).

Microscopic observation of cellular morphology in the coconut fruitlet abscission zone at different developmental time points

To further analyze the variation of cell architecture in AZ cells during fruitlet abscission, microscopic examination was conducted on AZ tissues from fruitlets destined to abscise and from those that persisted on the tree. The AZ cells, which are composed of small, densely cytoplasmic cells, were readily distinguishable in safranin-fast green-stained sections (Fig. 2).

The results showed that the AZ consisted of more than ten layers of regularly arranged, small, and compactly packed cells. In the CK group, the AZ contained relatively fewer cells, which appeared incompletely differentiated, tightly arranged, and rounded or elliptical in shape. These cells were conspicuously smaller than their neighboring cells and exhibited dense cytoplasm. The vascular tissues adjacent to the AZ appeared bright red in staining, contrasting sharply with the surrounding green parenchyma cells. The AZ cell walls remained intact, with no obvious intercellular space enlargement or cell wall degradation observed (Fig. 2A, B).

At 2 days after ethephon treatment, the AZ cells began to undergo pronounced morphological and structural changes. The cells enlarged in size, increased slightly in layer number, and elongated toward the middle region, accompanied by progressively enlarged intercellular spaces and loosened cell–cell connections. Numerous deposits appeared between cells, which may be associated with the formation of the protective layer at later stages of abscission (Fig. 2C, D). At 4 days after ethephon treatment, the fruitlets were observed to be in a state of partial abscission. The middle lamella between AZ cells had completely dissolved, leading to cell separation and the formation of a fracture surface. At this stage, cells around the fracture surface exhibited distorted

morphology, with some cells ruptured. Compared with the CK, extensive lignification was observed in cells at the AZ fracture surface, indicating that the tissue had already commenced preparation for protective layer formation following abscission. (Fig. 2E, F).

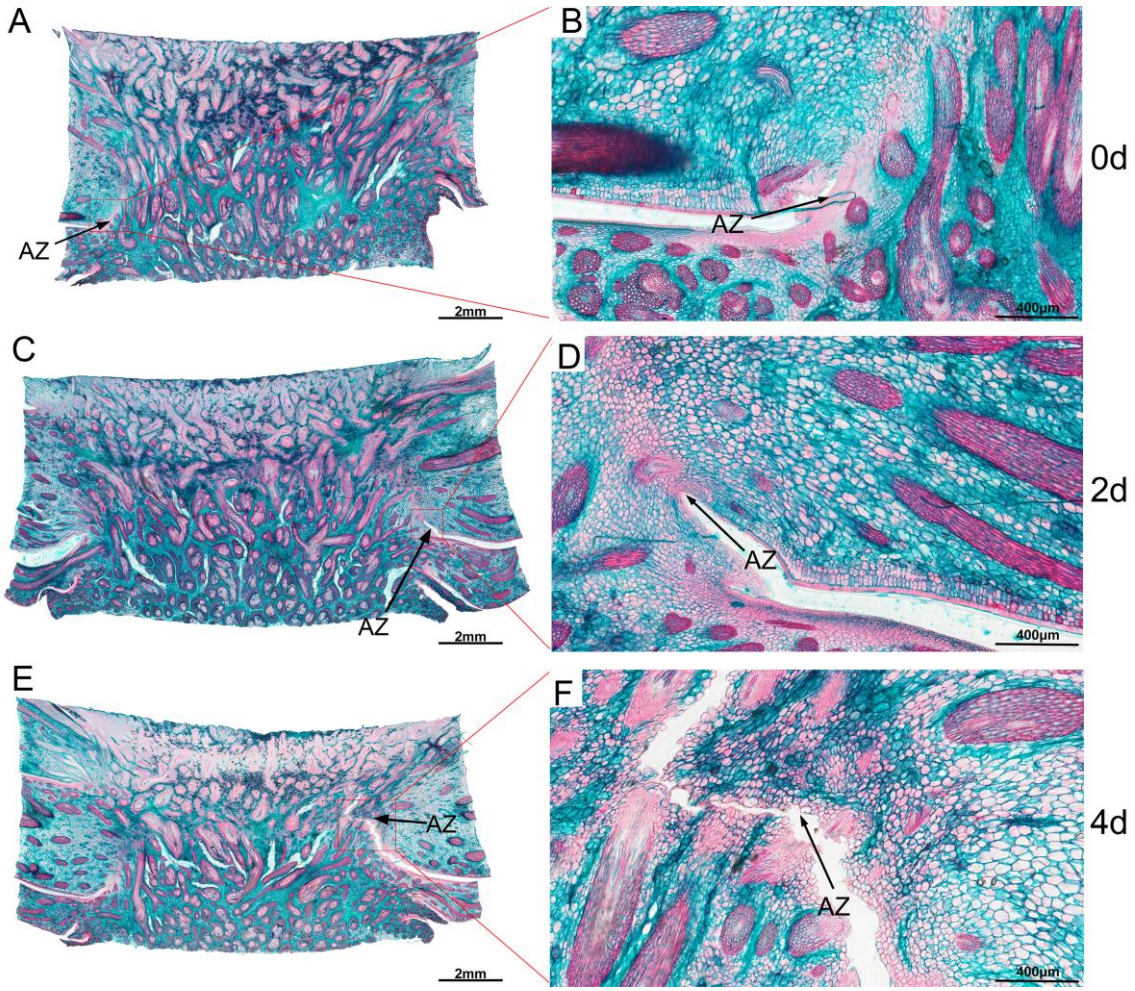


Fig. 2. Microstructural changes in the coconut fruitlet abscission zone after ethephon treatment.

A Abscission zone (AZ) and adjacent regions of non-abscised fruitlets under natural conditions; **B** Enlarged view of the red-boxed area in A; **C** AZ and adjacent regions of fruitlets at 2 days after ethephon treatment; **D** Enlarged view of the red-boxed area in C; **E** AZ and adjacent regions of fruitlets at 4 days after ethephon treatment; **F** Enlarged view of the red-boxed area in E.

Changes in Carbohydrate Levels During Fruitlet Abscission in Coconut

To assess whether carbohydrate metabolism is perturbed during ethephon-induced abscission, we quantified soluble sugar and starch contents in coconut fruitlets at 0, 2, and 4 days after treatment (Fig. 3). In the ethephon-treated group (ETH), the levels of total soluble sugars, glucose, fructose, and sucrose were consistently lower than those in the CK across all time points. Starch, however, showed the opposite trend: its content in the ETH group was markedly higher than in the CK group, suggesting a possible blockade in starch-to-sugar conversion under abscission-promoting conditions.

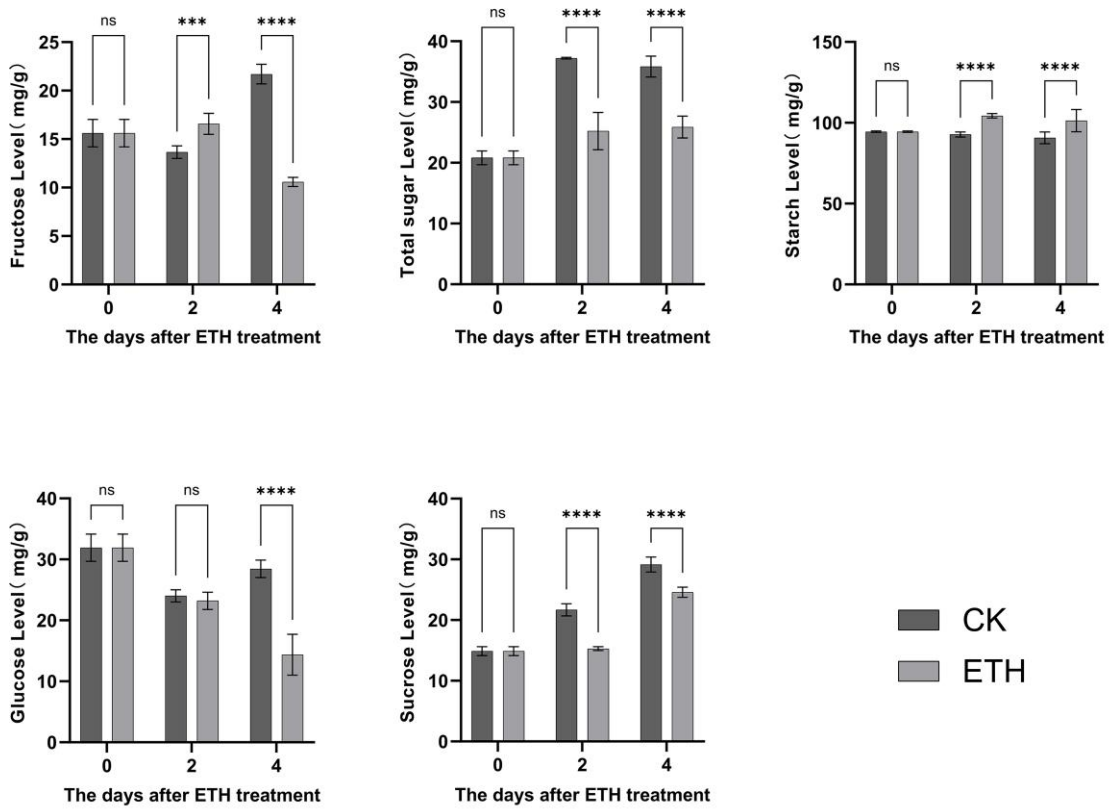
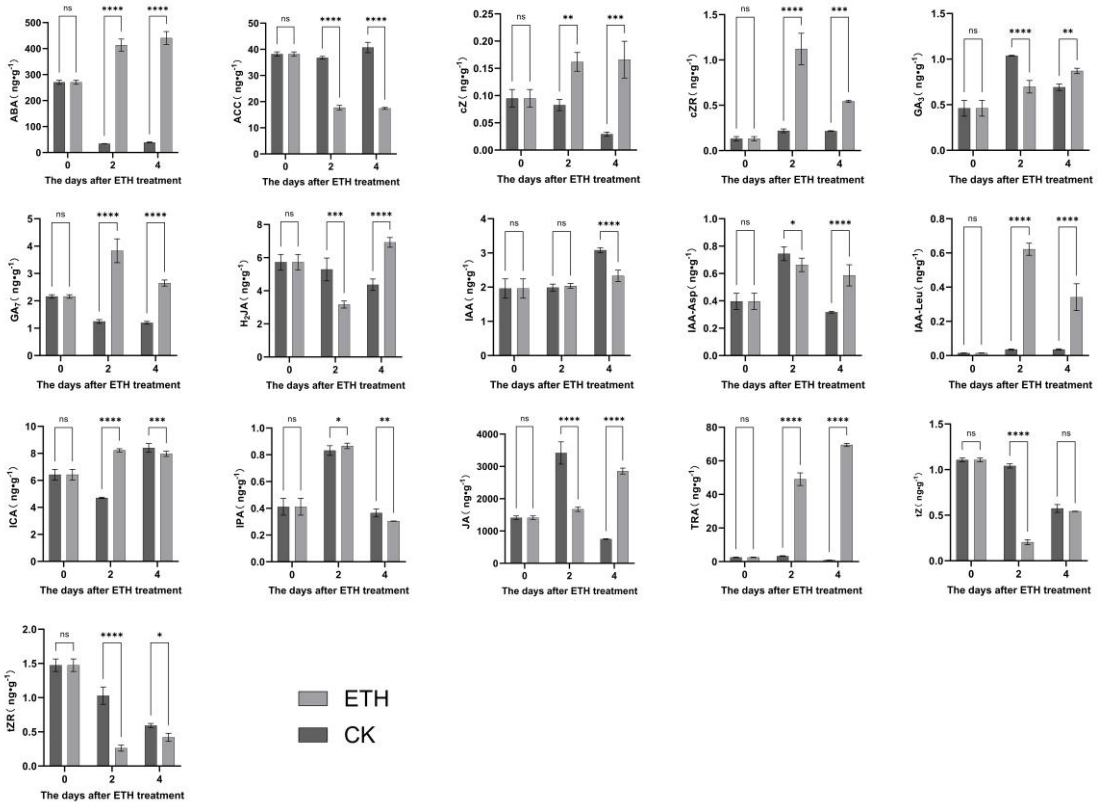


Fig. 3. Carbohydrate content differences in coconut fruitlets between ethephon-treated and control groups. *** and **** indicate significant differences from the CK group at $P < 0.001$ and $P < 0.0001$, respectively (Student's *t*-test). Error bars represent standard deviation (SD).

Changes in Phytohormone Levels During Fruitlet Abscission in Coconut

To elucidate the changes in phytohormones during fruitlet abscission in coconut, the endogenous phytohormone contents in the abscission zone of fruitlets were measured at 0, 2, and 4 days after ethephon treatment (Fig. 4). Among the auxin-class phytohormones, the contents of indole-3-acetic acid (IAA) and indole-3-carboxylic acid (ICA) in the ethephon-treated group (ETH) were higher than those in the control group (CK) at day 2, but were significantly lower than those in CK at day 4. The contents of the auxin biosynthesis precursors indole-3-propionic acid (IPA) and L-tryptophan (TRP) were significantly lower in ETH than in CK. In addition, the contents of several inactive auxin–amino acid conjugates (IAA-Asp and IAA-Leu) were found to be significantly higher in ETH than in CK.

Among the cytokinins (CTK), the contents of cis-zeatin (cZ) and cis-zeatin riboside (cZR) in ETH were significantly higher than those in CK, while the contents of trans-zeatin (tZ) and trans-zeatin riboside (tZR) were lower in ETH than in CK. For the gibberellins detected, the contents of GA_3 and GA_7 were significantly higher in ETH than in CK. The contents of jasmonic acid (JA) and dihydrojasmonic acid (H_2JA) in ETH were significantly lower than those in CK at day 2, but were significantly higher than those in CK at day 4. The content of abscisic acid (ABA) was substantially elevated in ETH. However, the content of the ethylene biosynthesis precursor 1-aminocyclopropane-1-carboxylic acid (ACC) was significantly lower in ETH than in CK.



184 **Fig. 4. Endogenous phytohormone contents in the coconut fruitlet abscission zone between ethephon-treated**

185 **and control groups.**

186 ABA, abscisic acid; ACC, 1-aminocyclopropane-1-carboxylic acid; cZ, cis-zeatin; cZR, cis-zeatin riboside; GA_3,

187 gibberellin A_3; GA_7, gibberellin A_7; H_2JA, dihydrojasmonic acid; JA, jasmonic acid; IAA, indole-3-acetic acid; ICA,

188 indole-3-carboxylic acid; IAA-Asp, IAA-aspartate (indole-3-acetyl-aspartic acid); IAA-Leu, IAA-leucine (indole-3-

189 acetyl-leucine); IPA, indole-3-propionic acid; TRP, L-tryptophan; tZ, trans-zeatin; tZR, trans-zeatin riboside. *, **,

190 ***, and **** indicate significant differences from the CK group at $P < 0.05$, $P < 0.01$, $P < 0.001$, and $P < 0.0001$,

191 respectively (Student's *t*-test). Error bars represent standard deviation (SD).

192 ## Digital Transcript Abundance Analysis

193 To identify key genes involved in fruitlet abscission, transcriptome sequencing was

194 performed on abscission zone samples collected from different treatment groups and at various

195 time points. The results showed that high-quality sequencing data were obtained for all samples

196 across the different treatment groups (CK vs. ETH) and time points (0, 2, and 4 days). The data
197 yield was consistent both between and within groups, with approximately 20 million reads per
198 sample. No N bases were detected in any of the samples, and the Q30 values ranged from 97.10%
199 to 99.23%. Samples from both the CK and ETH groups exhibited the highest sequencing accuracy
200 (mean Q30 > 99.10%). The GC content fluctuated within a narrow range of 46.00%–48.00%,
201 indicating stable sequencing performance without significant systematic bias and meeting the
202 requirements for subsequent differential expression analysis and other downstream analyses
203 (Supplementary Table S1).

204 **Identification of Differential Expression Genes Associated with Fruitlet Abscission**
205 **in Coconut Based on Transcriptomic Analysis**

206 Under the criteria of FDR < 0.05 and $|\log_2 FC| > 1$, comparative analysis between the CK2
207 vs. ETH2 and CK4 vs. ETH4 groups identified 887 and 1,561 DEGs, respectively (Fig. 5A, B).
208 Among these, in CK2 vs. ETH2, 556 genes were upregulated (62.68%) and 331 genes were
209 downregulated (37.32%); in CK4 vs. ETH4, 1,121 genes were upregulated (71.81%) and 440
210 genes were downregulated (28.19%). After removing redundant genes from these two sets, a total
211 of 2,195 DEGs were obtained, and GO and KEGG enrichment analyses were performed (Fig. 5C,
212 D). GO analysis revealed that these genes were classified into three categories: biological process,
213 cellular component, and molecular function. KEGG pathway analysis showed that these genes
214 were significantly enriched in the pathways of phytohormone signal transduction and plant–
215 pathogen interaction.

216 Subsequent analysis of these genes focused on those related to phytohormone biosynthesis

and signal transduction, cell wall modification, and transcription factors.

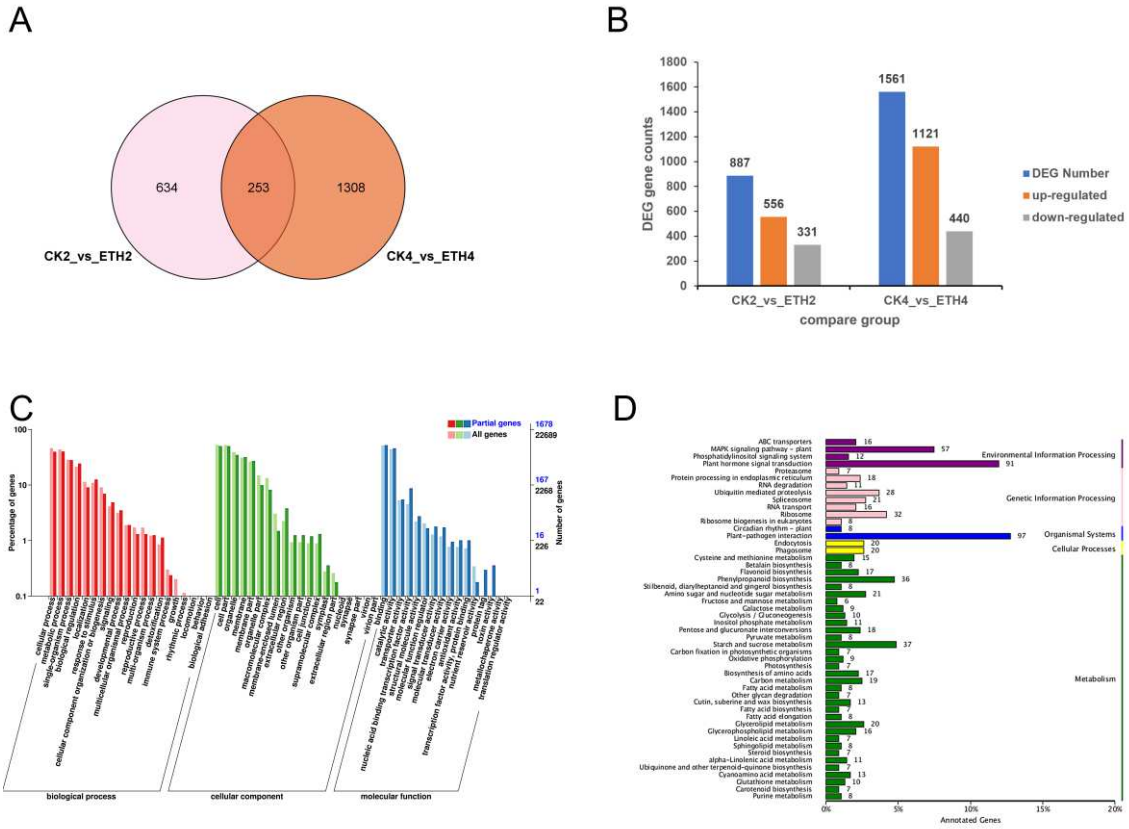


Fig. 5. Identification of DEGs in the coconut fruitlet abscission zone by transcriptomic analysis.

A Venn diagram of DEGs; **B** Bar plot of DEG statistics; **C** GO enrichment analysis; **D** KEGG pathway enrichment analysis.

Expression Patterns of Genes Related to Phytohormone Biosynthesis and Signal Transduction

Among the 2,195 DEGs identified above, a total of 75 genes were found to be associated with phytohormone biosynthesis and signal transduction (Supplementary Data 1). Among these, 51 genes were related to ethylene (ETH), 17 to IAA, and 7 to ABA (Fig. 6). Among the ethylene-related genes, 33 genes were significantly upregulated at 4 days after ethephon treatment, with most *ERF* family genes showing markedly increased expression at this time point. For auxin-

related genes, *ILR1*, *IAA10*, *SAUR32*, and *IAA1* were upregulated at 4 days after ethephon treatment. Notably, the expression of two auxin transporter genes, *PIN1* and *PIN6*, exhibited a downregulated trend over the course of ethephon treatment. Seven genes were associated with ABA, including the ABA receptor *PYL4* and ABA 8'-hydroxylase 1, among which *CYP707A1* and *NCED* showed significantly increased expression at 4 days after ethephon treatment. In addition, we observed that most *GH3*, *GH3.1 ACS*, and *ACO* genes were significantly upregulated at 4 days after ethephon treatment (Fig. 6B, C).

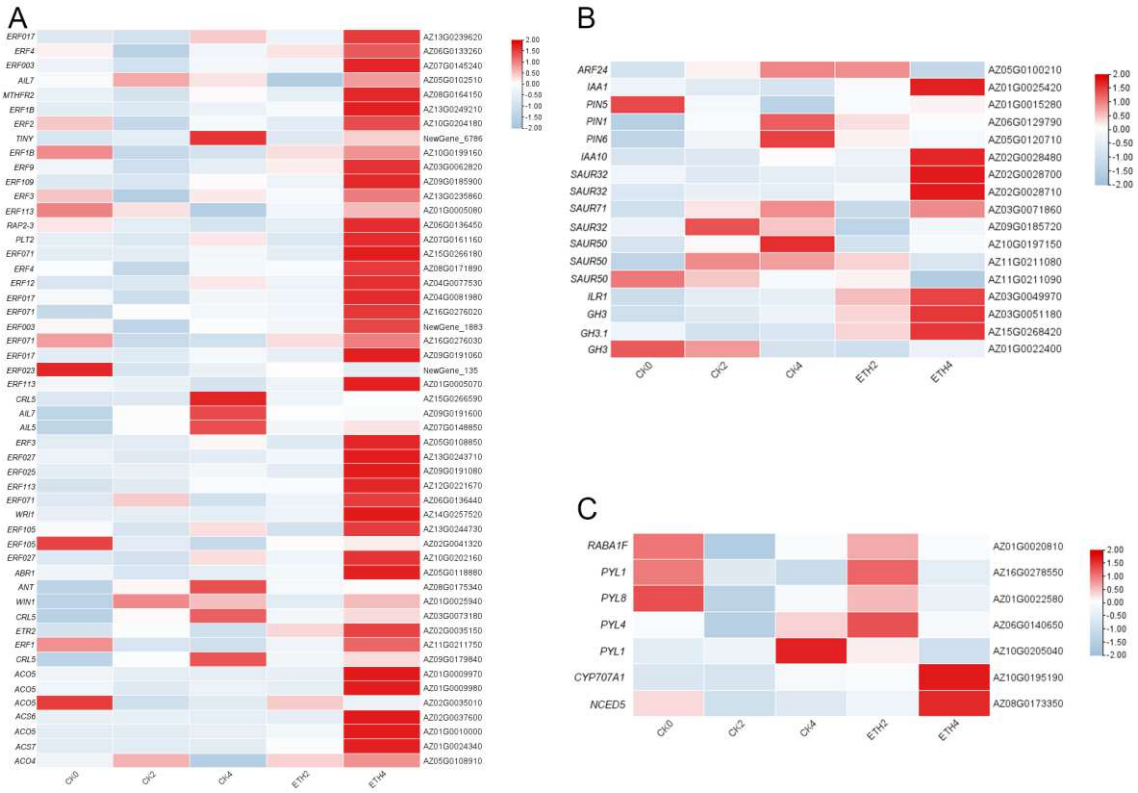


Fig. 6. Expression profiles of genes related to phytohormone biosynthesis and signal transduction.

A Ethylene-related genes; **B** Auxin-related genes; **C** Abscisic acid-related genes. Gene expression levels are indicated with color bars.

Expression Patterns of Genes Involved in Cell Wall Biosynthesis, Degradation, Loosening, and Remodeling

A total of 83 genes related to cell wall modification were identified (Supplementary Data 2), including 15 genes associated with cellulose metabolism, 33 with hemicellulose metabolism, 15 with pectin metabolism, 7 with Cell wall remodeling-related metabolism, and 13 with lignin metabolism (Fig. 7). Among the cellulose metabolism-related genes (Fig. 7A), the cellulose synthase gene *CSLH1* and the β-glucosidase gene *GLU14* showed upregulated expression in the ethephon-treated group, whereas the expression of *CSLE6*, *CSLD5*, *GLU11*, *GLU13*, and *GLU10* was suppressed compared with the control group. For hemicellulose metabolism-related genes (Fig. 7B), 27 genes were significantly upregulated at 4 days after ethephon treatment, while 6 genes were downregulated. These included xyloglucan endo-transglycosylase/hydrolase (*XTH*) and β-galactosidase (*BGAL*) genes.

Among the pectin metabolism-related genes (Fig. 7C), the expression of polygalacturonase (*PG*), polygalacturonase-inhibiting protein (*PGIP*), and pectin methyltransferase 2 (*QUA2*) was significantly upregulated at 4 days after ethephon treatment, whereas pectin methylesterase (*PME*) and pectin methylesterase inhibitor (*PMEI*) genes showed downregulated expression relative to the control group. Regarding lignin metabolism-related genes (Fig. 7D), which mainly included peroxidases (*PER*) and cinnamyl alcohol dehydrogenase (*CAD*) genes, the expression of *PER7*, *PER17*, *CAD6*, *SPC4*, *LAC6*, and *PERN* was significantly upregulated at 4 days after ethephon treatment, while *PER5* and *PER72* exhibited lower expression levels than those in the control group at the same time point.

In addition, seven genes involved in cell wall remodeling were identified (Fig. 7E), mainly encoding expansins, which function to loosen the cell wall of abscission zone cells, rendering the rigid wall structure “soft” and thereby facilitating the subsequent access of degradative enzymes such as polygalacturonase (PG) and cellulase (CEL) to the cell wall skeleton. Among these, four genes (*EXT2*, *EXPA11*, *LRX3*, and *EXPA4*) showed significantly higher expression levels than those in the control group, whereas *EXRA16* expression was significantly lower than that in the control group.

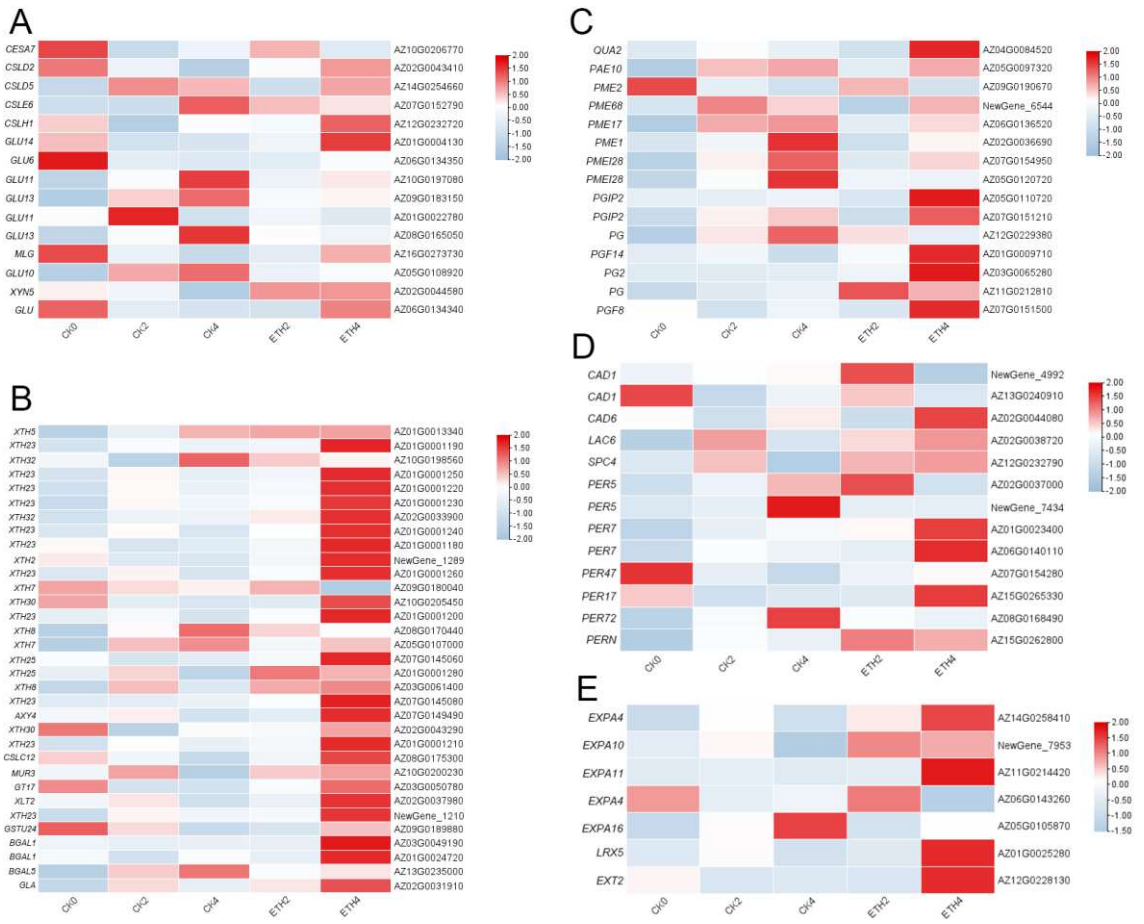


Fig. 7. Expression profiles of genes related to cell wall modification.

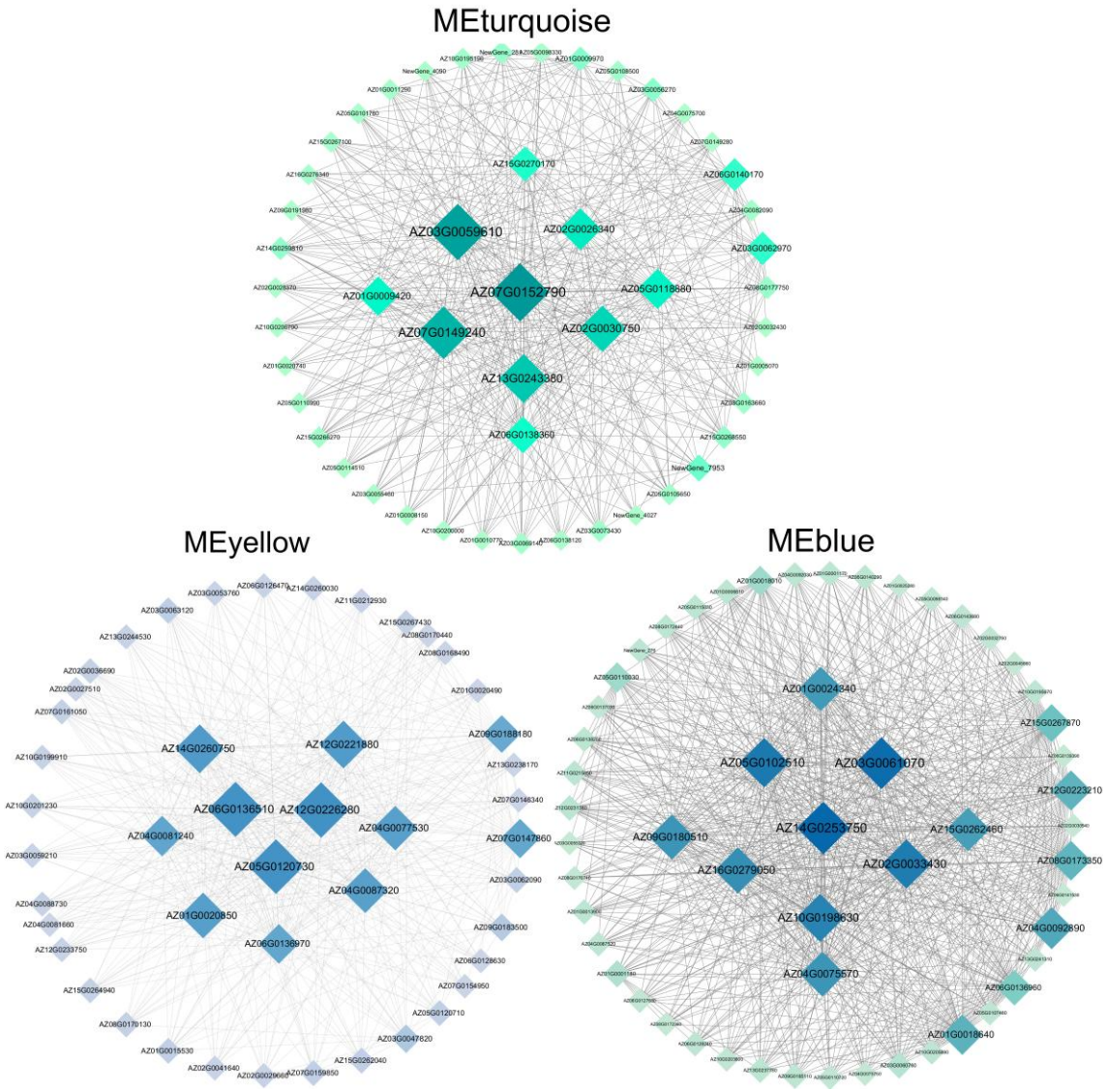
A Cellulose metabolism-related genes; B, Hemicellulose metabolism-related genes; **C** Pectin metabolism-related genes; **D** Lignin metabolism-related genes; **E** Cell wall remodeling-related genes. Gene expression levels are indicated with color bars.

WGCNA Analysis Elucidating the Potential Mechanisms Underlying Fruitlet Abscission in Coconut

To investigate the correlations between genes and phenotypic traits, weighted gene co-expression network analysis (WGCNA) was performed on the 2,195 DEGs in conjunction with fruit abscission rate (FAR) and the contents of IAA, ABA, ACC, and JA. During the WGCNA procedure, the soft-thresholding power was first determined using the pickSoftThreshold function. As shown in Fig. S1A, when the power value reached 11, the correlation coefficient (R^2) approached a plateau, indicating that the network approximated a scale-free topology. Based on similar expression patterns, a total of six co-expression modules were identified (Fig. S1B, C), and the number of genes in each module is provided in Supplementary Data 3.

The results showed that the blue module was significantly negatively correlated with ACC and significantly positively correlated with ABA (Fig. S1 C); the turquoise module was significantly positively correlated with abscission rate; the green module was significantly positively correlated with ABA; and the yellow module was significantly positively correlated with IAA. From the blue, turquoise, and yellow modules, which exhibited significant trait correlations, we selected genes with potential functional relevance (KME $\geq$ 0.9, GS $\geq$ 0.7) to construct co-expression networks (Fig. 8). In these networks, node size represented the connectivity degree of each gene, and the ten genes with the highest connectivity were positioned at the network center, serving as hub genes. Functional characterization of these genes may further elucidate their regulatory roles in the fruitlet abscission process of coconut.

Subsequently, functional annotation was performed for the 30 identified hub genes (Supplementary Data 4) to explore their potential roles during fruitlet abscission. In the yellow module, we identified an ethylene-responsive transcription factor (ERF) gene (*AZ04G0077530*), an endoglucanase-encoding gene (*AZ06G0136510*), an LRR receptor-like serine/threonine-protein kinase ERECTA-encoding gene (*AZ04G0081240*), and *CYP71A1* (*AZ12G0226280*), a gene encoding a key enzyme in the gibberellin biosynthesis pathway. In the blue module, we identified *ACS7* (*AZ01G0024340*) involved in ethylene biosynthesis, *CYP94A1* (*AZ09G0180510*) related to jasmonic acid metabolism, an AP2-like ethylene-responsive transcription factor gene (*AZ05G0102510*), and an aldehyde reductase gene (*AZ04G0075570*) associated with ABA synthesis. In the turquoise module, we identified an ethylene-responsive factor ABR1 gene (*AZ05G0118880*), a serine/threonine-protein kinase-like protein CCR4 gene (*AZ01G0009420*), a β-glucanase gene (*AZ07G0149240*), and an NADH dehydrogenase gene (*AZ03G0059610*) involved in ROS production. These genes are speculated to play critical roles during fruitlet abscission in coconut.



306 **Fig. 8. Co-expression network construction and hub gene identification in WGCNA modules.**

307 Genes with KME ≥ 0.9 and GS ≥ 0.7 were selected for network visualization. Node size represents gene connectivity,

308 and the ten most highly connected genes (hub genes) are positioned at the network center.

309

Transcription Factor-Encoding Genes

Among the 2,195 DEGs, 196 were assigned to 14 transcription factor families, including ERF/AP2, WRKY, NAC, bHLH, MYB, HD-ZIP, GRAS, GRF, HSF, bZIP, ZF-HD, MADS, NIL, and TFIID (Fig. 9). The ERF/AP2 family was the most prevalent and exhibited the most pronounced expression changes among all families identified, with 15 and 31 genes upregulated and 2 and 8 genes downregulated in the CK2 vs. ETH2 and CK4 vs. ETH4 comparisons, respectively. The WRKY family exhibited a comparable upregulation pattern, with 5 and 22 genes upregulated and 2 and 1 genes downregulated in the two comparisons, respectively. Notably, all NAC family genes identified in this study were upregulated (Supplementary Data 5).

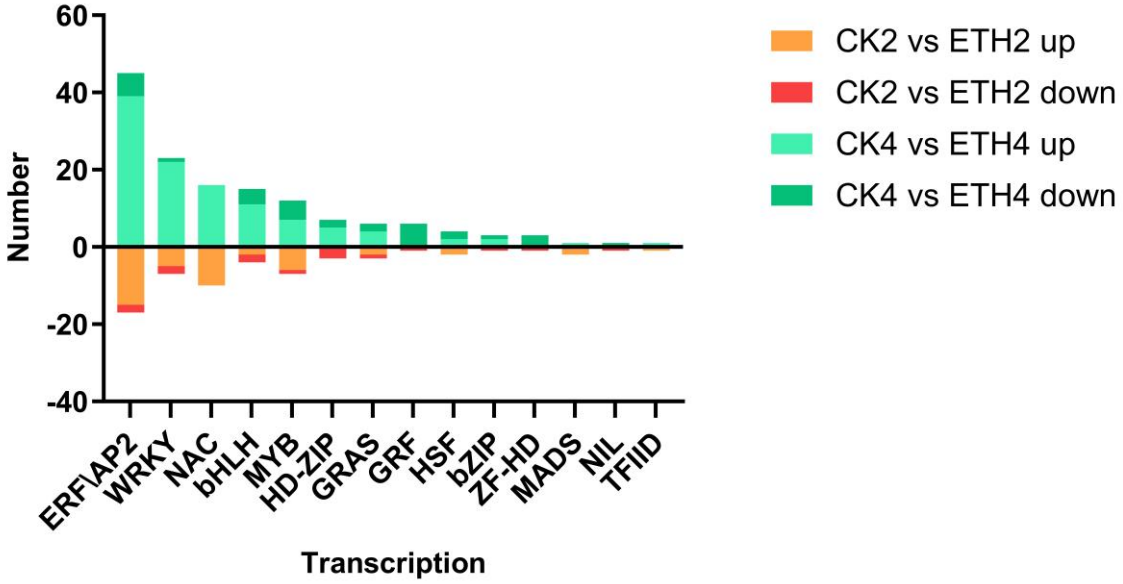


Fig. 9. Transcription factor-encoding genes identified from the DEGs.

The 14 transcription factor families are shown, with upregulated and downregulated genes indicated for the CK2 vs. ETH2 and CK4 vs. ETH4 comparisons. All NAC family genes were upregulated.

Validation of Gene Expression Patterns by qRT-PCR

To validate the expression patterns of the aforementioned DEGs, 17 randomly selected genes were analyzed by quantitative real-time PCR (qRT-PCR) (Fig. 10). The results demonstrated that the expression patterns of the validated genes were highly consistent with those detected by RNA-seq, confirming the reliability of the transcriptomic data.

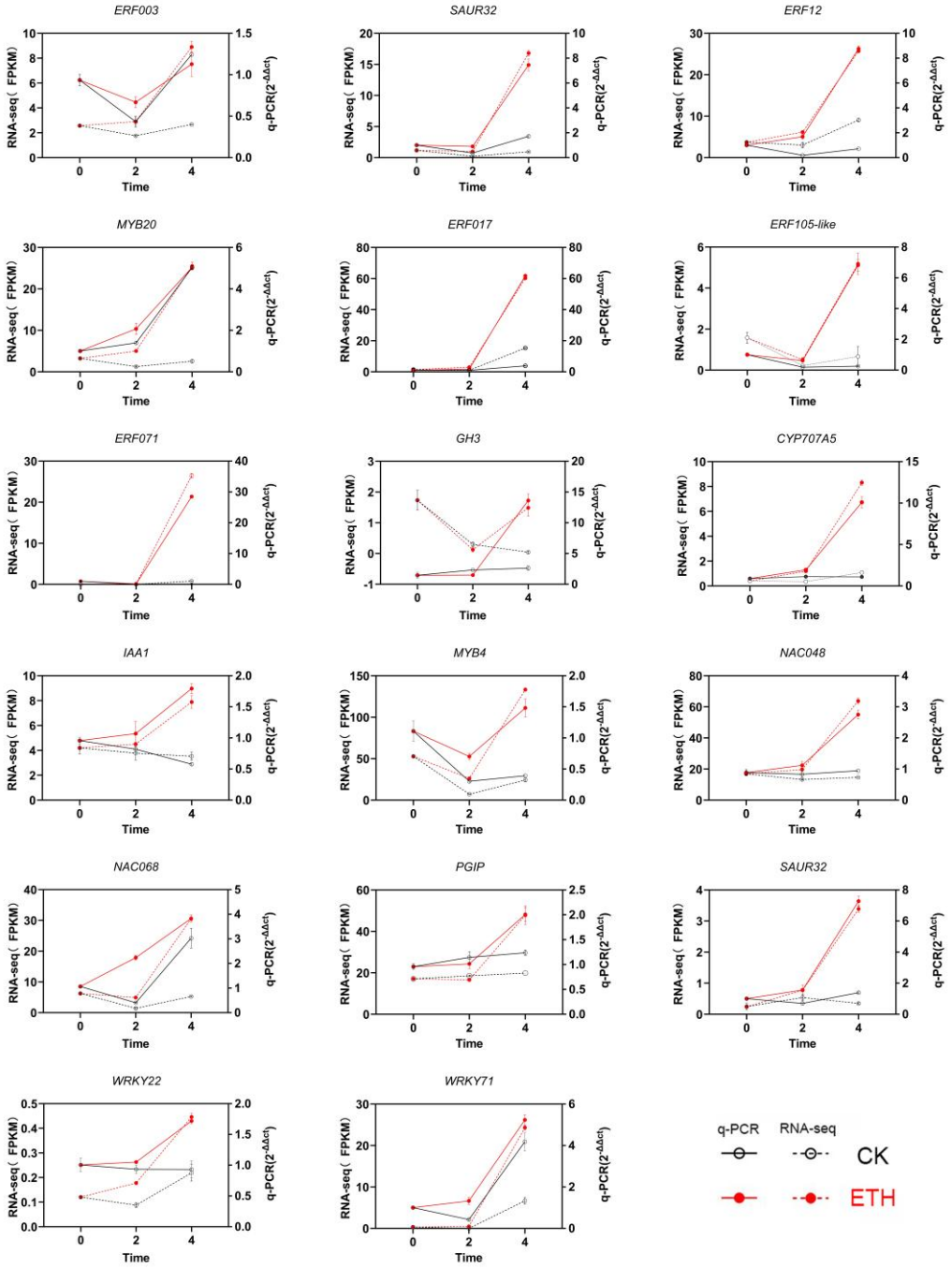


Fig. 10. qRT-PCR validation of the expression patterns of 17 selected abscission-associated genes.

Discussion

Fruitlet abscission in coconut is a complex physiological process governed by a sophisticated molecular regulatory network that integrates both external environmental cues and internal developmental signals. Previous studies have demonstrated that ethylene induces organ abscission in plants [28], and ethephon, a plant growth regulator that releases ethylene, is widely used in agricultural production to promote or simulate fruit abscission [29]. In the present study, we simulated ethylene-induced abscission by exogenous ethephon application and integrated cytological, physiological, biochemical, and transcriptomic evidence to systematically characterize the dynamic changes occurring in the coconut fruitlet abscission zone (AZ) throughout the abscission process.

Carbohydrates serve a dual function in abscission, acting both as energy substrates and as signaling molecules. In litchi, restricted carbohydrate supply triggers fruitlet abscission when pedicel glucose levels drop below a critical threshold [30], and sugar starvation promotes fruit drop via activation of ABA and ethylene accumulation coupled with disruption of IAA transport [31]. Our results showed that total sugars, fructose, sucrose, and glucose in the AZ of ethephon-treated fruits were significantly lower than those in the control group. This reduction may reflect an interruption of carbohydrate nutrient supply following the receipt of abscission signals, leading to rapid consumption of accumulated sugars and thereby facilitating fruit shedding[32]. Notably, starch content in the treated group was higher than in the control group (Fig. 3), a pattern opposite to that observed in most plant species. We speculate that this anomalous accumulation results from a blockage in the conversion of starch to soluble sugars, although the underlying mechanism warrants further investigation. Impaired carbohydrate metabolism may not only compromise

energy supply and signaling but also intersect with cell wall degradation and remodeling in the AZ. In *Elymus sibiricus*, genotypes with high seed-shattering rates exhibited earlier degradation of the abscission layer and lower lignin content in the abscission zone compared with low-shattering genotypes [33]. However, our anatomical observations revealed that lignification in the coconut fruitlet AZ increased progressively with prolonged ethephon treatment, as indicated by enhanced safranin staining, and a distinct fracture surface appeared at 4 days post-treatment (Fig. 2E, F). We propose that this structural transition marks the acquisition of complete separation capacity by the AZ, and that the formation of a lignified protective layer is an adaptive strategy to prevent pathogen invasion and protect the wound surface after abscission [34].

The interplay among phytohormone signaling networks is recognized as the core driver of organ abscission [35], with the antagonistic balance between auxin and ethylene directly determining the timing of abscission initiation. In soybean, abscission-prone varieties exhibited elevated auxin–amino acid conjugate levels, upregulation of *GH3* genes, and downregulation of *PIN* family genes, collectively disrupting the auxin concentration gradient in the AZ [15]. In *Arabidopsis*, specific reduction of auxin levels in the floral organ AZ similarly led to premature abscission [36]. Our study observed an identical regulatory pattern in coconut fruitlets: free IAA content in the AZ of the ethephon-treated group decreased significantly at day 4, accompanied by elevated levels of multiple auxin–amino acid conjugates (Fig. 4), as well as upregulation of *GH3* and *GH3.1* and downregulation of *PIN1*, *PIN5*, and *PIN6* (Fig. 6B). These findings are consistent with the notion that ethylene reduces bioactive IAA levels by inhibiting polar auxin transport or promoting auxin conjugation[37].

Auxin depletion, in turn, enhances the sensitivity of the AZ to ethylene[38]. Extensive

evidence has established the role of ethylene in plant organ abscission. As the terminal effector of this process, ethylene directly triggers cell wall degradation via activation of downstream transcription factor cascades [11]. In tomato, for example, ethylene treatment upregulated *TAPG* expression in both the AZ and the distal abaxial region during ethylene-induced abscission, and the resulting increase in PG activity led to dissolution of the middle lamella, cell separation, and eventual pedicel abscission [39]. Furthermore, genes involved in ethylene biosynthesis and signaling function as key regulators of organ abscission across diverse plant species. In litchi, the transcription factors LcEIL2 and LcEIL3 mediate fruitlet abscission through positive regulation of ethylene synthesis genes and cell wall-degrading enzyme genes [40]. In *Areca catechu* L., the ethylene-responsive transcription factor AcERF116 was highly expressed in the fruit AZ, and its overexpression in tomato accelerated cell separation and promoted abscission [22]. These observations collectively demonstrate that transcription factors downstream of the ethylene signaling pathway are key regulators of fruit abscission. In our study, ethylene signaling-related genes, including *ERF* and *ABR1*, were upregulated in the treated group, further supporting the central role of this pathway in regulating coconut fruitlet abscission. Notably, ACC content decreased progressively with treatment duration, while expression of the ACC oxidase genes *ACO*, which catalyze the conversion of ACC to ethylene, was upregulated in the ETH group. We attribute this decline to accelerated consumption of ACC as the direct precursor of ethylene synthesis during active abscission.

Beyond the classical auxin–ethylene regulatory axis, other phytohormones also contribute to abscission regulation through distinct mechanisms. Cytokinins (CTK) have been reported to promote abscission, although high concentrations may inhibit the process [41]. In rose petal

abscission, bioactive cytokinins accumulated during shedding and functioned as promoting factors [26]. In our study, most cytokinin components were elevated in the treated group, whereas *trans*-zeatin and its riboside exhibited a decreasing trend. We hypothesize that tZ and tZR, which were present at substantially higher levels than other CTKs in the coconut AZ, may play an inhibitory role, and their decline over time may represent a prerequisite for relieving inhibition and accelerating abscission. However, the precise mechanism requires further investigation.

Gibberellins (GA) exhibit more complex and species-specific effects. In mango, exogenous GA_3, auxin analogs, or cytokinin analogs improved fruit retention and yield [32]. In poplar axillary buds, GA_3 and GA_4 exerted opposing functions, promoting abscission and activating growth, respectively [42]. These findings suggest that the role of GA in abscission may vary across species or depend on the organ involved. In our study, GA_3 and GA_7 contents were significantly elevated in the treated group. However, given that gibberellins are also broadly involved in stress responses, whether their elevation directly promotes abscission or merely reflects a general stress response remains to be determined.

Abscisic acid (ABA) is widely recognized as a factor that promotes cell separation, but it does not directly trigger abscission; rather, it acts indirectly by promoting senescence and mediating stress responses[43]. ABA can induce ACC accumulation, stimulate ethylene synthesis, and thereby accelerate shedding of aged or damaged tissues[37]. In our study, ABA content was significantly higher in the treated group than in the control, accompanied by high expression of the key biosynthesis gene *NCED*, consistent with a synergistic role in amplifying ethylene signals. Jasmonic acid (JA), although primarily associated with stress responses, also functions as a

positive regulator of abscission. JA signaling can reduce IAA content by inhibiting IPA-mediated IAA biosynthesis, thereby lowering auxin concentration in the AZ and promoting abscission[7]. Ethylene-insensitive receptors can respond to JA signals to accelerate abscission, and mutants defective in either JA synthesis ((*AOS*, *OPR3* mutants) or perception (*coi1* mutant) both exhibited delayed floral organ abscission, confirming JA as a positive regulator [44]. In our study, JA content in the ETH group was significantly higher than in the CK group at day 4, consistent with these previous findings.

Conclusions

In this study, ethephon treatment promoted coconut fruitlet abscission and induced clear cytological changes in the abscission zone. The combined carbohydrate and phytohormone analyses indicate that abscission is associated with impaired carbohydrate metabolism and hormonal imbalance, particularly ethylene burst and auxin depletion. Transcriptome analysis further identified DEGs and hub genes related to phytohormone signaling, cell wall modification, and transcriptional regulation. These findings support the conclusion that ethephon-induced fruitlet abscission in coconut is driven by the combined effects of carbohydrate impairment and hormonal imbalance, which trigger transcriptional reprogramming, cell wall degradation, and cell separation. This study provides a theoretical basis for coconut fruit abscission and identifies candidate genes for fruit tree breeding.

Materials and Methods

Plant Materials and Treatments

The coconut (*Cocos nucifera* L.) cultivar "Wenye No. 2" was used in this study. Trees were grown at a spacing of 6 m × 6 m in the experimental field of the Coconut Research Institute, Chinese Academy of Tropical Agricultural Sciences, in Wenchang, Hainan, China. Nine trees of uniform vigor were randomly selected and assigned to three biological replicates (three trees per replicate). Ethephon treatment (2 g/L) was applied to inflorescences immediately after female flower pollination, following the protocol of Chen et al. (2024), in which this concentration induced complete fruit abscission within 4 days with consistent rates across replicates. Each inflorescence was split into two halves: one half was sprayed with the ethephon solution and bagged, while the other half was treated with water and bagged as the control. Both solutions contained 0.05% (v/v) Tween 20 (Sangon Biotech Co., Ltd., Shanghai, China) as a surfactant and were delivered using a manual sprayer. At 0, 2, and 4 days post-treatment, abscission zone tissues (approximately 2 mm thick) were excised from fruitlets with a razor blade. One portion was immediately frozen in liquid nitrogen and stored at −80°C for RNA extraction, transcriptome sequencing, and biochemical assays; the other portion was fixed for histological analysis of the abscission zone. For abscission rate measurements, an additional nine trees of comparable vigor and flowering stage were treated identically, and the number of dropped fruits was recorded at 0, 2, and 4 days after treatment. The abscission rate was calculated according to the following formula: Abscission rate (%) $= {}^{x_t}/_{x_0} \times 100$, where x_t is the number of abscised fruits at time (t) and x_0 is the initial fruit set number.

Microscopic Observation of Abscission Zone Cells

Abscission zone tissues were collected at 0, 2, and 4 days after ethephon treatment, immediately fixed in FAA fixative solution (formalin–acetic acid–alcohol) for 24 hours, and then stored in 70.00% ethanol at 4°C until further processing. Fixed samples were dehydrated through a graded ethanol series, cleared in xylene, and embedded in paraffin wax. Serial sections of 8–10 μm thickness were cut using a rotary microtome and mounted onto glass slides. Sections were dewaxed, rehydrated, and stained with safranin–fast green according to standard protocols (Sass, 1958). Stained sections were dehydrated, cleared, and mounted with neutral balsam. Observations and photomicrography were performed using a light microscope (Olympus BX53, Olympus Corporation, Tokyo, Japan). Cellular morphology, encompassing aspects such as cell size, arrangement, intercellular spaces, and wall integrity, was assessed in the abscission zone and neighboring regions at each time point.

Determination of Carbohydrate Content in coconut fruitlets

Coconut fruitlets collected at 0, 2, and 4 days after ethephon treatment, as well as those from the water-treated control group at the corresponding time points, were used for carbohydrate content determination. Fructose content was measured using the Solarbio Fructose Content Assay Kit (BC2455, micro-method). Total sugar content was measured using the Solarbio Total Sugar Content Assay Kit (BC2715, micro-method). Sucrose content was measured using the Solarbio Sucrose Content Assay Kit (BC2465, micro-method). Glucose content was measured using the Solarbio Glucose Content Assay Kit (BC2505, micro-method). Starch content was measured using the Solarbio Starch Content Assay Kit (BC0705, micro-method). All assays were performed

according to the manufacturer's instructions. Three biological replicates were performed for each indicator, with three technical replicates per biological replicate.

Determination of Endogenous Phytohormone Contents in the Abscission Zone

Abscission zone tissues of coconut fruitlets collected at 0, 2, and 4 days after ethephon treatment, as well as those from the water-treated control group at the corresponding time points, were used for determination of endogenous phytohormone contents. The contents of abscisic acid (ABA), 1-aminocyclopropane-1-carboxylic acid (ACC), cis-zeatin (cZ), cis-zeatin riboside (cZR), gibberellin A_3 (GA_3), gibberellin A_7 (GA_7), dihydrojasmonic acid (H_2JA), jasmonic acid (JA), indole-3-acetic acid (IAA), indole-3-carboxylic acid (ICA), IAA-aspartate (IAA-Asp), IAA-leucine (IAA-Leu), indole-3-propionic acid (IPA), L-tryptophan (TRP), trans-zeatin (tZ), and trans-zeatin riboside (tZR) were measured according to the method of Li et al. (2023). The abscission zone tissues were ground to a fine powder in liquid nitrogen, and pre-cooled acetonitrile–water solution was added for ultrasonic-assisted extraction. After centrifugation, the supernatant was collected. The extract was purified using reverse-phase solid-phase extraction (RP-SPE) cartridges: the SPE cartridges were sequentially pre-conditioned with methanol and distilled water and equilibrated with acetonitrile–water solution. After sample loading, the cartridges were washed with an appropriate solvent, and the target fractions were collected. The eluate was dried, and the residue was reconstituted in acetonitrile, transferred to sample vials, and subjected to ultra-high-performance liquid chromatography–tandem mass spectrometry (UHPLC-MS/MS) analysis. Data acquisition and processing were performed using SCIEX Analyst Work Station Software (Version 1.6.3) and SCIEX OSQ software, respectively.

Transcriptome Analysis

Total RNA was extracted from three biological replicates of the CK0, CK2, CK4, ETH2, and ETH4 groups using Trizol reagent. cDNA library construction, Illumina sequencing, and subsequent data processing followed the method of Li et al. (2022) [45]. For functional annotation, the assembled transcripts were aligned against the NCBI non-redundant protein sequence database (NR), Clusters of Orthologous Groups (KOG/COG), Gene Ontology (GO), UniProt Knowledgebase Swiss-Prot (Swiss-Prot), and the Kyoto Encyclopedia of Genes and Genomes (KEGG). Gene expression levels were calculated as FPKM (fragments per kilobase of transcript per million mapped reads). Differentially expressed genes (DEGs) were identified using a false discovery rate (FDR) < 0.05 and $|\log_2 (\text{fold change})| \geq 1$ as the thresholds. Weighted gene co-expression network analysis (WGCNA) was performed with R 4.6.0, and the resulting networks were visualized using Cytoscape v3.10.3.

Quantitative Real-Time PCR Analysis

Total RNA from samples of the CK and ETH groups was reverse-transcribed into cDNA using the PrimeScript™ RT Reagent Kit (TaKaRa, Japan). qRT-PCR was performed using the Applied Biosystems QuantStudio 3 & 5 Real-Time PCR System (Thermo Fisher Scientific, China). The reaction mixture consisted of 5 μL PowerUp SYBR Green Master Mix (Applied Biosystems, USA), 1 μL cDNA, 1 μL forward primer, 1 μL reverse primer, and 2 μL double-distilled water (ddH_2O). The thermal cycling protocol was as follows: initial denaturation at 95°C for 2 min; 40 cycles of denaturation at 95°C for 15 s and annealing/extension at 60°C for 1 min; followed by melt curve analysis of 95°C for 15 s, 60°C for 60 s, and 95°C for 15 s. The relative

expression levels of each sample were calculated using the $2^{-\Delta\Delta CT}$ method, normalized to the Ct values of the internal reference gene. All experiments were performed with three independent biological replicates. The coconut *Actin* gene was used as the internal reference for data normalization, and the qRT-PCR primers were designed using FastPCR 5.3.76 software, with primer sequences provided in Supplementary Table S2. The primers were synthesized by Shanghai Sangon Biotech Co., Ltd.

Data Processing

Data processing was performed using Microsoft Excel 2021, and figures were generated using TBtools-II (Version 2.450) and GraphPad Prism 11.

Statistical Analysis

All experiments were performed with at least three biological replicates, and statistical significance was analyzed using Student's t-test.

Acknowledgements

We would like to express our gratitude to the staff of the Coconut Research Institute of Chinese Academy of Tropical Agricultural Sciences and the workers at the germplasm resources nursery for their support and assistance with this experiment.

Authors' contributions

WF conceived and designed this study. WF wrote the manuscript. WF performed most of the experiments. JL, LW, ML and LL cultivated and prepared the plants for RNA sequencing. All authors have reviewed and approved the final manuscript.

Funding

This work was supported by the Natural Science Foundation of China (32672426) and the National Key R&D Program of China (2023YFD2200700).

Availability of data and materials

The transcriptome data has been deposited into the China National Center for Bioinformation with the code CRA050474 (https://ngdc.cncb.ac.cn/gsa/search?searchTerm=CRA050474).

Declarations

Ethics approval and consent to participate

The authors declare that all the permissions or licenses were obtained to collect the *Cocos nucifera* L. and that all study complies with relevant institutional, national, and international guidelines and legislation for plant ethics in the methods section.

Consent for publication

Not applicable.

Competing interests

The authors declare no competing interests.

References

1. Qi MF, Xu T, Chen WZ, Li TL. Ultrastructural localization of polygalacturonase in ethylene-stimulated abscission of tomato pedicel explants. Scientific World Journal. 2014;2014:389896.

2. Estornell LH, Agustí J, Merelo P, Talón M, Tadeo FR. Elucidating mechanisms underlying organ abscission. Plant Sci. 2013;199-200:48-60.

3. Li J, Chen Y, Zhou G, Li M. Phytohormones and candidate genes synergistically regulate fruitlet abscission in *Areca catechu* L. BMC Plant Biol. 2023;23:537.

4. Jackson MB, Osborne DJ. Abscisic Acid, Auxin, and Ethylene in Explant Abscission. J Exp Bot. 1972;23:849-862.

5. Ren B, Zhang L, Chen J, Wang H, Bian C, Shi Y, Qin D, Huo J, Gang H. Response of Abscission Zone of Blue Honeysuckle (*Lonicera caerulea* L.) Fruit to GA3 and 2,4-D Spray Application. Agronomy. 2023;13:2937.

6. Wu H, He Q, He B, He S, Zeng L, Yang L, Zhang H, Wei Z, Hu X, Hu J et al. Gibberellin signaling regulates lignin biosynthesis to modulate rice seed shattering. Plant Cell. 2023;35:4383-4404.

7. Wu X, Cao Y, Chen Y, Xiong W, Cao G, Zeng Y, Zhang L, Zeng R, Chen D. Integration of transcriptome and phytohormone analyses reveals antagonistic interactions between jasmonate and auxin signaling pathways in rice (*Oryza sativa* L.). Front Plant Sci. 2025;16:1622785.

8. Ueda J, Miyamoto K, Hashimoto M. Jasmonates promote abscission in bean petiole expiants: Its relationship to the metabolism of cell wall polysaccharides and cellulase activity. J Plant

578 Growth Regul. 1996;15:189-195.
579 9. Furuta Y, Yamamoto H, Hirakawa T, Uemura A, Pelayo MA, Iimura H, Katagiri N, Takeda-
580 Kamiya N, Kumaishi K, Shirakawa M et al. Petal abscission is promoted by jasmonic acid-
581 induced autophagy at Arabidopsis petal bases. Nat Commun. 2024;15:1098.
582 10. Zhu L, Yu H, Xu X, Yu Z. Postharvest application of methyl jasmonate inhibited ethylene
583 biosynthesis and signaling in peach through activating the negative feedback of JA-signaling
584 pathway. Postharvest Biol Technol. 2024;213:112965.
585 11. Xu J, Chen L, Sun H, Wusiman N, Sun W, Li B, Gao Y, Kong J, Zhang D, Zhang X et al.
586 Crosstalk between cytokinin and ethylene signaling pathways regulates leaf abscission in
587 cotton in response to chemical defoliants. J Exp Bot. 2019;70:1525-1538.
588 12. Mor Y, Spiegelstein H, Halevy AH. Inhibition of ethylene biosynthesis in carnation petals by
589 cytokinin. Plant Physiol. 1983;71:541-546.
590 13. Liu XD, Zeng YY, Hasan MM, Ghimire S, Jiang H, Qi SH, Tian XQ, Fang XW. Diverse
591 functional interactions between ABA and ethylene in plant development and responses to
592 stress. Physiol Plant. 2024;176:e70000.
593 14. Li J, Li M, Wang L, Wan Y. An AcDOF4-AcPILS7 Module Promotes Fruitlet Abscission by
594 Suppressing Auxin Transport in *Areca catechu* L. Plant Cell Environ. 2025;48:6209-6212.
595 15. Tan Z, Han W, Mao W, Wang X, Li S, Luan X, Yao X, Guo K, Xie F. Transcriptome and
596 Targeted Hormone Metabolome Reveal the Mechanism of Flower Abscission in Soybeans
597 Under Shade. Int J Mol Sci. 2025;26:10303.
598 16. Sawicki M, Aït Barka E, Clément C, Vaillant-Gaveau N, Jacquard C. Cross-talk between
599 environmental stresses and plant metabolism during reproductive organ abscission. J Exp

Bot. 2015;66:1707-1719.

17. Ma C, Jiang C-Z, Gao J. Regulatory Mechanisms Underlying Activation of Organ Abscission. In: Annu Plant Rev Online. 2021; 27-56.

18. Fan L, Zhou W, Shang S, Zhou S, Gao S, Shaaban M, Wang Z, Shi G. Deciphering the auxin-ethylene crosstalk in petal abscission through auxin influx carrier IpAUX1 of Itoh peony 'Bartzella'. Postharvest Biol Technol. 2024;216:113060.

19. Agustí M, Martínez-Fuentes A, Mesejo C, Marzal A, Reig C. Expression of carbohydrate-related genes underlying 3,5,6-TPA-induced fruitlet abscission in citrus. Sci Rep. 2024;14:26482.

20. Li C, Zhao M, Ma X, Wen Z, Ying P, Peng M, Ning X, Xia R, Wu H, Li J. The HD-Zip transcription factor LcHB2 regulates litchi fruit abscission through the activation of two cellulase genes. J Exp Bot. 2019;70:5189-5203.

21. Ma X, He Z, Yuan Y, Liang Z, Zhang H, Lalun VO, Liu Z, Zhang Y, Huang Z, Huang Y et al. The transcriptional control of LcIDL1-LcHSL2 complex by LcARF5 integrates auxin and ethylene signaling for litchi fruitlet abscission. J Integr Plant Biol. 2024;66:1206-1226.

22. Li J, Chen Y, Wang L, Li D, Liu L, Li M. An ethylene response factor AcERF116 identified from *A. catechu* is involved in fruitlet abscission. Plant Sci. 2024;344:112091.

23. Mao L, Begum D, Chuang HW, Budiman MA, Szymkowiak EJ, Irish EE, Wing RA. JOINTLESS is a MADS-box gene controlling tomato flower abscission zone development. Nature. 2000;406:910-913.

24. Galindo-Trigo S, Bågman AM, Ishida T, Sawa S, Brady SM, Butenko MA. Dissection of the IDA promoter identifies WRKY transcription factors as abscission regulators in Arabidopsis.

622 J Exp Bot. 2024;75:2417-2434.
623 25. Chen J, Jiang S, Yang G, Li L, Li J, Yang F. The MYB transcription factor SmMYB113
624 directly regulates ethylene-dependent flower abscission in eggplant. Plant Physiol Biochem.
625 2024;209:108544.
626 26. Jiang C, Liang Y, Deng S, Liu Y, Zhao H, Li S, Jiang CZ, Gao J, Ma C. The RhLOL1-
627 RhILR3 module mediates cytokinin-induced petal abscission in rose. New Phytol.
628 2023;237:483-496.
629 27. Rajapakse CNK, Wijesekaea HTR, Norman AH. A preliminary study on immature nutfall of
630 coconut with reference to pest damage. COCOS. 2010;10:53-54.
631 28. Tipu MMH, Sherif SM. Ethylene and its crosstalk with hormonal pathways in fruit ripening:
632 mechanisms, modulation, and commercial exploitation. Front Plant Sci. 2024;15:1475496.
633 29. Ish Shalom M, Sadowsky A, Tikochinsky T, Ostrovsky Y, Adler-Agmon M, Cohen Y.
634 Effects of Ethrel and auxin applications on date palm fruit abscission during development. Sci
635 Hortic. 2024;326:112755.
636 30. Yi JW, Ge HT, Abbas F, Zhao JT, Huang XM, Hu GB, Wang HC. Function of a non-
637 enzymatic hexokinase LcHXK1 as glucose sensor in regulating litchi fruit abscission. Tree
638 Physiol. 2023;43:130-141.
639 31. Zhao K, Gao Z, Zhang X, Li S, Hong Q, Li H, Li F, Shi H, Wang J. Sugar signaling-
640 mediated hormonal regulatory networks: molecular mechanisms underlying fruit abscission
641 and development in seedless litchi. BMC Plant Biol. 2025;25:1535.
642 32. Jones SC, Orr R, Rossouw GC, Smith HM, Beveridge CA, Shaw LM. Insights into the
643 molecular regulation of premature fruit drop - what we have learned from mango (*Mangifera*

644 *indica*) and other fruit crops. Sci Hortic. 2026;355:114572.
645 33. Xie W, Zhang J, Zhao X, Zhang Z, Wang Y. Transcriptome profiling of Elymus sibiricus, an
646 important forage grass in Qinghai-Tibet plateau, reveals novel insights into candidate genes
647 that potentially connected to seed shattering. BMC Plant Biol. 2017;17:78.
648 34. Rascio N, Casadoro G, Ramina A, Masia A. Structural and biochemical aspects of peach
649 fruit abscission (*Prunus persica* L. Batsch). Planta. 1985;164:1-11.
650 35. Pautot V, Crick J, Hepworth SR. Abscission zones: cellular interfaces for the programmed
651 separation of organs. Ann Bot. 2025;136:29-48.
652 36. Basu MM, González-Carranza ZH, Azam-Ali S, Tang S, Shahid AA, Roberts JA. The
653 manipulation of auxin in the abscission zone cells of Arabidopsis flowers reveals that
654 indoleacetic acid signaling is a prerequisite for organ shedding. Plant Physiol. 2013;162:96-
655 106.
656 37. Kućko A, Wilmowicz E, Tranbarger TJ. Editorial: Phytohormones as crucial players in
657 organ abscission. Front Plant Sci. 2025;16:1716731.
658 38. Meir S, Philosoph-Hadas S, Sundaresan S, Selvaraj KSV, Burd S, Ophir R, Kochanek B,
659 Reid MS, Jiang C-Z, Lers A. Microarray Analysis of the Abscission-Related Transcriptome in
660 the Tomato Flower Abscission Zone in Response to Auxin Depletion. Plant Physiol.
661 2010;154:1929-1956.
662 39. Jiang CZ, Lu F, Imsabai W, Meir S, Reid MS. Silencing polygalacturonase expression
663 inhibits tomato petiole abscission. J Exp Bot. 2008;59:973-979.
664 40. Ma X, Yuan Y, Wu Q, Wang J, Li J, Zhao M. LcEIL2/3 are involved in fruitlet abscission via
665 activating genes related to ethylene biosynthesis and cell wall remodeling in litchi. Plant J.

2020;103:1338-1350.

41. Pierik RLM, Abbadi SAB. The effect of cytokinins on auxin-induced secondary abscission in isolated apple pedicels. Z Pflanzenphysiol. 1972;68:281-282.

42. Katyayini NU, Rinne PLH, Tarkowská D, Strnad M, van der Schoot C. Dual Role of Gibberellin in Perennial Shoot Branching: Inhibition and Activation. Front Plant Sci. 2020;11:736.

43. Finkelstein RR, Rock CD. Abscisic Acid biosynthesis and response. Arabidopsis Book. 2002;1:e0058.

44. Kim J. Four shades of detachment: regulation of floral organ abscission. Plant Signal Behav. 2014;9:e976154.

45. Li J, Jia X, Yang Y, Chen Y, Wang L, Liu L, Li M. Genome-Wide Identification of the DOF Gene Family Involved in Fruitlet Abscission in *Areca catechu* L. Int J Mol Sci. 2022;23:11768.

Figure Legends

Fig. 1. Morphological characteristics of the abscission zone and fruitlets in coconut.

A Comparison of inflorescences treated with water (CK) or ethephon (ETH); **B** Non-abscised fruitlet; **C** Abscised fruitlet; **D** Abscission rate of coconut fruitlets. **** indicates significant differences from the CK group at $P<0.0001$ (Student's *t*-test). Error bars represent standard deviation (SD).

Fig. 2. Microstructural changes in the coconut fruitlet abscission zone after ethephon treatment.

A Abscission zone (AZ) and adjacent regions of non-abscised fruitlets under natural conditions; **B** Enlarged view of the red-boxed area in A; **C** AZ and adjacent regions of fruitlets at 2 days after ethephon treatment; **D** Enlarged view of the red-boxed area in C; **E** AZ and adjacent regions of fruitlets at 4 days after ethephon treatment; **F** Enlarged view of

the red-boxed area in E.

Fig. 3. Carbohydrate content differences in coconut fruitlets between ethephon-treated and control groups.

*** and **** indicate significant differences from the CK group at $P < 0.001$ and $P < 0.0001$, respectively (Student's *t*-test). Error bars represent standard deviation (SD).

Fig. 4. Endogenous phytohormone contents in the coconut fruitlet abscission zone between ethephon-treated and control groups.

ABA, abscisic acid; ACC, 1-aminocyclopropane-1-carboxylic acid; cZ, cis-zeatin; cZR, cis-zeatin riboside; GA_3, gibberellin A_3; GA_7, gibberellin A_7; H_2JA, dihydrojasmonic acid; JA, jasmonic acid; IAA, indole-3-acetic acid; ICA, indole-3-carboxylic acid; IAA-Asp, IAA-aspartate (indole-3-acetyl-aspartic acid); IAA-Leu, IAA-leucine (indole-3-acetyl-leucine); IPA, indole-3-propionic acid; TRP, L-tryptophan; tZ, trans-zeatin; tZR, trans-zeatin riboside. *, **, ***, and **** indicate significant differences from the CK group at $P < 0.05$, $P < 0.01$, $P < 0.001$, and $P < 0.0001$, respectively (Student's *t*-test). Error bars represent standard deviation (SD).

Fig. 5. Identification of DEGs in the coconut fruitlet abscission zone by transcriptomic analysis.

A Venn diagram of DEGs; **B** Bar plot of DEG statistics; **C** GO enrichment analysis; **D** KEGG pathway enrichment analysis.

Fig. 6 Expression profiles of genes related to phytohormone biosynthesis and signal transduction.

A Ethylene-related genes; **B** Auxin-related genes; **C** Abscisic acid-related genes. Gene expression levels are indicated with color bars.

Fig. 7. Expression profiles of genes related to cell wall modification.

A Cellulose metabolism-related genes; B, Hemicellulose metabolism-related genes; **C** Pectin metabolism-related genes; **D** Lignin metabolism-related genes; **E** Cell wall remodeling-related genes. Gene expression levels are indicated with color bars.

Fig. 8. Co-expression network construction and hub gene identification in WGCNA modules.

Genes with KME ≥ 0.9 and GS ≥ 0.7 were selected for network visualization. Node size represents gene connectivity, and the ten most highly connected genes (hub genes) are positioned at the network center.

Fig. 9. Transcription factor-encoding genes identified from the DEGs.

The 14 transcription factor families are shown, with upregulated and downregulated genes indicated for the CK2 vs. ETH2 and CK4 vs. ETH4 comparisons. All NAC family genes were upregulated.

Fig. 10. qRT-PCR validation of the expression patterns of 17 selected abscission-associated genes.

Authors and Affiliations

Wenlong Fan[1, 2], Wencheng Fan[1, 2], Linkai Wang[2], Liyun Liu[2], Meng Li[1, 3, *], Jia Li[2, *]

[1]College of Life Science and Technology, Central South University of Forestry and Technology, Changsha, 410004, China

[2]Coconut Research Institute, Chinese Academy of Tropical Agricultural Sciences, Wenchang, 571339 Hainan China

[3]Yuelushan Laboratory, Changsha, Hunan 410128, China

[*]Corresponding author: Meng Li (limeng0422@csuft.edu.cn), Jia Li (lijiali027@163.com).

Supplementary Files

This is a list of supplementary files associated with this preprint. Click to download.

- SupplementaryData.zip